FERMILAB-PUB-11-292-AE

Mon. Not. R. Astron. Soc. **000**, 000–000 (0000) Printed 22 June 2011 (MN LATEX style file v2.2)

The architecture of the hierarchical triple star KOI 928 from eclipse timing variations seen in *Kepler* photometry

J. H. Steffen[1⋆], S. N. Quinn[2], W. J. Borucki[3], E. Brugamyer[4], S. T. Bryson[3], L. A. Buchhave[5] W. D. Cochran[4], M. Endl[4], D. C. Fabrycky[6], E. B. Ford[7], M. J. Holman[2], J. Jenkins[3,8], D. Koch[3], D. W. Latham[2], P. MacQueen[4], F. Mullally[3,8], A. Prša[9], D. Ragozzine[2], J. F. Rowe[3], D. T. Sanderfer[3], S. E. Seader[3,8] D. Short[10], A. Shporer[11], S. E. Thompson[3,8], G. Torres[2], J. D. Twicken[3,8] W. F. Welsh[10], G. Windmiller[10]

[1] *Fermilab Center for Particle Astrophysics, P.O. Box 500, Batavia, IL 60510, USA*
[2] *Harvard-Smithsonian Center for Astrophysics, 60 Garden St., Cambridge, MA 02138, USA*
[3] *NASA Ames Research Center, Moffett Field, CA 94035, USA*
[4] *McDonald Observatory, The University of Texas, Austin, TX 78712-2059, USA*
[5] *Niels Bohr Institute, Copenhagen University, DK-2100 Copenhagen, Denmark*
[6] *Department of Astronomy and Astrophysics, University of California, Santa Cruz, Santa Cruz, CA 95064, USA*
[7] *Department of Astronomy, University of Florida, 211 Bryant Space Science Center, Gainesville, FL 32611-2055, USA*
[8] *SETI Institute, 515 North Whisman Road, Mountain View, CA, 94043*
[9] *Villanova University, Department of Astronomy and Astrophysics, 800 E. Lancaster Ave., Villanova, PA 19085*
[10] *San Diego State University, 5500 Campanile Drive, San Diego, CA 92182, USA*
[11] *Las Cumbres Observatory Global Telescope, Goleta, CA 93117, USA*

22 June 2011

ABSTRACT

We present a hierarchical triple star system (KIC 9140402) where a low mass eclipsing binary orbits a more massive third star. The orbital period of the binary (4.98829 Days) is determined by the eclipse times seen in photometry from NASA's *Kepler* spacecraft. The periodically changing tidal field, due to the eccentric orbit of the binary about the tertiary, causes a change in the orbital period of the binary. The resulting eclipse timing variations provide insight into the dynamics and architecture of this system and allow the inference of the total mass of the binary ($0.424 \pm 0.017 M_{\odot}$) and the orbital parameters of the binary about the central star.

Key words: Eclipsing Binaries, *Kepler*, KIC 9140402, FERMILAB-PUB-11-292-AE

1 INTRODUCTION

The timings of transit or eclipse events in multibody astronomical systems provide a high precision measurement of the phase of the orbits of the transiting bodies—typically a few parts in 10^4 or better. Such high precision measurements allow for detailed studies of the dynamics of these systems through eclipse timing variations or ETVs (or transit timing variations, TTVs, for planetary systems) (Borkovits et al. 2003; Agol et al. 2005; Holman and Murray 2005). A variety of mechanisms can cause the eclipse times to deviate from a linear ephemeris including the Rømer effect (light travel time, or LTT), transverse displacements of the star with respect to the system barycentre, resonance interactions among the bodies, and effects that correspond to the synodic periods of the objects. A detailed discussion of these cases is found in Agol et al. (2005).

One notable cause of ETVs is the effect of a changing tidal field on a binary pair due to a perturber on a hierarchical, eccentric orbit. This scenario was derived analytically in Borkovits et al. (2003) and a simplified derivation is shown in Agol et al. (2005). Basically, when the perturbing third object is far from its short-period binary companions, the period of the binary is largely unmodified. However, when the perturbing object is near the binary and near the binary's orbital plane, its presence slows the orbital period of the binary. The result is a periodic TTV signal with a period equal to the orbit time of the perturbing body. The more eccentric the orbit, the larger and more asymmetric the TTV signal appears because the slowing of the binary's orbital

⋆ E-mail: jsteffen@fnal.gov

Operated by Fermi Research Alliance, LLC under Contract No. DE-AC02-07CH11359 with the United States Department of Energy.

period at the perturber's pericentre passage takes a smaller fraction of its orbital period and the large change in proximity from the high eccentricity exaggerates the change in the binary's period. The nature of this signal is such that it is virtually independent of the azimuthal orientation of the apse of the orbit of the perturbing body, though it does depend upon the mutual inclination of the two relevant orbital planes.

The first system known to exhibit this effect, also found with *Kepler* photometric data, is the triple star system KOI 646 (KIC 5384802, Fabrycky 2010). Here we present and discuss a second stellar system that shows a periodic ETV signal consistent with this same model, KOI 928 (KIC 9140402). A third *Kepler* system that shows similar orbital architecture, but that is viewed in a different orientation—and thus does not show the same ETV signal, is KOI 126 (KIC 5897826, Carter et al. 2011). Additional star systems that show trends indicative of dynamical interactions were reported in Slawson et al. (2011). The paper is organized as follows. In Section 2 we present the *Kepler* photometry and transit times. In Section 3 we outline the spectroscopically derived stellar parameters and radial velocity (RV) measurements of the target star. Section 4 gives the dynamical analysis of the transit times and radial velocity measurements of the system. Concluding remarks are in Section 5. We note that the true orbital structure of these systems is a bright central star orbited by an eclipsing binary of low mass stars. However, for the purposes of our discussion we will label the eclipsing binary as the "inner binary" of objects one and two and the third star, which perturbs the orbital period of the inner binary, as the third or "outer" object.

2 *Kepler* PHOTOMETRY

KOI 928 (KIC 9140402) has *Kepler* magnitude Kp = 15.251, making it quite dim among *Kepler* targets. It is located at RA 18:59:02.26 and Dec 45:35:56.86. For our study, we use data from the first six quarters of *Kepler* operations (BJD 2454968 – 2455650) corresponding to nearly 700 days of observation. Information about the *Kepler* spacecraft and its performance can be found in Koch et al. (2010). The period of the eclipse events is 4.98829 Days and the eclipse depths are 0.06% of the nominal flux. A binned lightcurve and representative model (generated using the PHOEBE software from Prša and Zwitter (2005)), is shown in Figure 1.

This system was initially identified as a planetary candidate through the Transiting Planet Search and the Data Validation Pipelines (Jenkins et al. 2010; Wu et al. 2010) which identify significant transit-like features and conduct a battery of statistical tests on those transit events in an effort to rule out false-positive transit signals. As data for KOI 928 were being analyzed, the interpretation of the system quickly grew complicated. The transit times showed a sizeable, roughly sinusoidal timing variations with nearly a two-hour peak-to-peak amplitude (consistent with a near-resonant two-planet system). However, intial RV measuremen nts (described in the next section) differed significantly from the predictions of a two-planet model.

A PSF fit to the difference image formed by subtracting averaged in-transit pixels from averaged out-of-transit pixels (see Torres et al. 2011) indicated no significant centroid motion. This fact effectively eliminates the possibility of the transits being on a star that is more distant than 0.3 pixels (1.2") from KOI-928. Taken together, with a few additional RV data, the information suggests a model of a bright star being orbited by a low-mass binary pair.

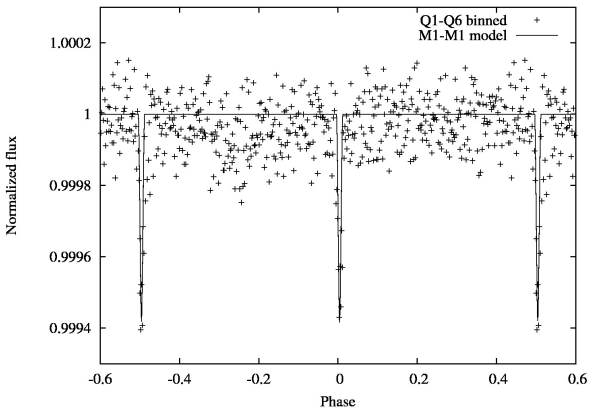

Figure 1. Binned and folded light curve for KOI 928. Also shown is a representative model which has equal size ($R = 0.238R_\odot$) and mass ($M = 0.21M_\odot$) members of the binary.

Attempts to model the eclipse times of this system suffer both from the lack of photons (given the dimness of the target) as well as additional systematic errors. In particular, some estimates of the eclipse times show multiple local minima while others have unusually large error bars. Consequently, we derived the eclipse times and their uncertainties using two different methods (described below). We then adopt one set of times as "nominal", but eliminate eclipses at certain epochs based upon the estimated errors and the differences between the two methods. Times from the second method are not analyzed in the dynamical model.

To estimate the nominal eclipse times for both the members of the eclipsing binary, we fit standard $4^{\rm th}$ order nonlinear limb-darkened eclipse models (Mandel and Agol 2002) to the Kepler light curve. For each primary or secondary eclipse, the model allowed for independent values of the primary-secondary radius ratio, eclipse duration, and impact parameter. For each eclipse, we fit for the flux normalization and a local linear slope in the flux and we numerically average the model over the 30 minute integration duration.

The first step to determine the eclipse times is to fit a single model to the set of all eclipses for each individual star assuming a constant orbital period. Second, we hold the radius ratio, eclipse duration, and impact parameter fixed, and fit a small segment of the light curve around each eclipse for the remaining parameters. Third, we phase the light curve using each measured eclipse and refit for the eclipse parameters (aside from period and epoch). The second and third steps are iterated to converge on a final model. This model also includes a nuisance parameter which estimates the "contamination" light from stars in the Kepler aperture (excluding the star being eclipsed) as a fixed parameter. We verified that our results for eclipse times are not sensitive to the value of this nuisance parameter.

The second, comparative set of eclipse time estimates were calculated using an iterative process starting with an initial linear ephemeris and eclipse width. Eclipses in the

"raw" data were masked, then the light curve was piecewise detrended and normalized locally (0.5 days) using a cubic polynomial. All the eclipses were then folded on the ephemeris, and a piecewise cubic Hermite spline was fitted using least-squares to the folded eclipse using observations that fell within a window of width 1.4× the eclipse width + 1 cadence on each side. The cubic Hermite spline was fit using 9 evenly spaced points across the window and the χ^2 of the fit recorded. The cubic Hermite was refit 25 more times using odd numbers (11-35) of spline knots. The best fit from these 26 cases defined the eclipse template, and the eclipse width estimate was updated using this template.

The light curve was again detrended locally using a cubic polynomial but now using three different out-of-eclipse lengths: 7.5 hours, 15 hours, and 20 hours. For each of the three out-of-eclipse lengths, the template was correlated with the eclipse at 1000 time steps, spanning 115 min. The estimate for the mid-eclipse time is that which gave the minimum χ^2 value over the three different out-of-eclipse lengths.

This entire process was iterated using the new eclipse time estimates, but those eclipses with a reduced $\chi^2 > 2.0$ were eliminated from the template building step, and the correlation time step length was reduced by a factor of 8. Once the second iteration was completed, the uncertainties in eclipse times were estimated using the χ^2 curve of the fits.

To select the eclipse times from the nominal (first) method to used in our analysis, we rejected those epochs where either of the two methods had large uncertainties (greater than 0.045 days) and the epochs where the two methods disagree by more than 3σ. The epochs that survive these cuts were analyzed. These two criteria were determined by analyzing the distribution of the differences in the eclipse times of the two models and the distribution of the uncertainties in the eclipse times. In both cases (the cut on uncertainty and the cut on difference) there is an obvious gap where the outlier population dominates over the nominal distribution and the chosen cuts reflect those transitions. The eclipse times used for this analysis are given in the appendix.

3 STELLAR PROPERTIES, IMAGING, AND SPECTROSCOPIC OBSERVATIONS

We obtained seven high-resolution spectra of KOI 928 in order to measure improved stellar properties of the bright, outer star and to place radial velocity constraints on its orbit. Six spectra were taken with the Tull Coudé Spectrograph on the 2.7m Harlan J. Smith Telescope at the McDonald Observatory in west Texas, which has a resolving power of $R \approx 60,000$ and wavelength coverage $3750 - 10000$ Å. One additional spectrum was taken with the Fiber-fed Echelle Spectrograph (FIES) on the 2.5m Nordic Optical Telescope (NOT) at La Palma, Spain (Djupvik and Andersen 2010). The FIES spectrum was taken with the medium-resolution fiber, which has resolving power of $R \approx 46,000$ and wavelength coverage $3600 - 7400$ Å.

In order to determine the effective temperature ($T_{\rm eff}$), projected rotational velocity ($v \sin i$), surface gravity ($\log g$), and metallicity ([Fe/H]) of the bright star in the system, we cross-correlated the strongest spectrum—the only one with signal-to-noise ratio (SNR) greater than 20 per resolution element—against a grid of synthetic stellar spectra computed from Kurucz models (Kurucz 1992). A new set of tools (Buchhave et al. 2011) was then used to derive more precise stellar parameters from the normalized cross correlation peaks. Formally, the value of $\log g = 4.56$ places the star below the isochrones in an unphysical part of the H-R diagram. This is most likely due to errors in the measured quantities and given the relatively low SNR of our spectrum and the strong spectroscopic correlations between $T_{\rm eff}$, $\log g$, and [Fe/H], this is not surprising. However, the formal error in $\log g$ is large enough that there are valid solutions that do fall on the isochrones. The results from this analysis, with conservative uncertainties, are given in Table 1.

Table 1. Stellar parameters for the central star in KOI 928.

Parameter	Value	Uncertainty
$T_{\rm eff}(K)$	5506	150
$\log g$	4.56	0.23
$[Fe/H]$	0.08	0.29
Vsini (km/s)	3.3	1.7
M_3 ($M_\odot$)	0.97	0.1
R_3 ($R_\odot$)	0.89	0.1

Table 2. Radial velocity measurements.

Date (BJD - 2454900)	Radial Velocity (km/s)	Error (km/s)	Instrument
445.8325	-8.039	0.339	MCD
523.5395	10.322	0.400	FIES
570.6033	-14.269	0.319	MCD
596.6075	-4.859	0.343	MCD
599.6062	-2.119	0.340	MCD
627.5932	11.821	0.319	MCD
732.9574	9.697	0.520	MCD

To obtain radial velocities, we performed a multi-order cross-correlation of the six McDonald spectra following the procedure outlined in Buchhave et al. (2010). For the FIES spectrum, we adopt the RV derived from cross-correlation against the best-matched synthetic template. The velocities are shifted onto the IAU absolute scale as defined by the velocity of the IAU RV standard HD 182488 (Nidever et al. 2002). The errors have been inflated to include an instrumental component corresponding to the long term RMS velocity residuals of HD 182488 as observed by each instrument. The RV measurements derived from this analysis are given in Table 2.

4 DYNAMICAL MODEL

As discussed above, the case of a hierarchical triple system where the distant third body is on an eccentric orbit, the changing tidal field produced by the perturbing third body causes a change in the period of the binary that cycles with its orbit about the perturber. For our investigation, we use the coplanar approximation as model fits with mutually inclined orbits did not produce a sufficent improvement to justify the additional parameters. Thus, our model is given

by (equation (25) in Agol et al. (2005)):

$$\delta t = \xi \frac{P_3}{(1-e_3^2)^{3/2}} \left[f_3 - \frac{2\pi(t-\tau_3)}{P_3} + e_3 \sin f_3 \right] \quad (1)$$

where

$$\xi \equiv \frac{1}{2\pi} \left(\frac{m_3}{m_1+m_2} \right) \left(\frac{P_{12}}{P_3} \right)^2 \quad (2)$$

and where m_1 and m_2 are the masses of the two objects in the binary, P_{12} is the period of the binary. The parameters for the third body are its mass m_3, period P_3, eccentricity e_3, time of pericentre passage τ_3, and true anomaly f_3 (we change notation from Agol et al. (2005) to use the "3" subscript to denote the third body). The ETV effect for this coplanar case is independent of the orientation of the orbit of the third body with respect to the observer (i.e., the longitude of pericentre ϖ_3). This orientation can be measured through the LTT effect and with the RV data. For KOI 928, the timing uncertainties are too large to provide meaningful contraints from LTT alone and require the inclusion of RV measurements in the analysis to identify the value of this parameter.

The seven model parameters for our analysis include the mass ratio $M \equiv m_3/(m_1+m_2)$, P_{12}, P_3, τ_3, e_3, ϖ_3, and the ephemeris epoch T_0 in BJD-2454900. The mass ratio is not well constrained by the transit data without an estimate for one of the masses (either the mass of the perturber or the mass of the binary). Consequently, we fix the mass of the pertuber to the value determined from the spectroscopy.

The RV data and timing data were fit to the ETV model in equation 1, with additional terms for the geometric LTT effect and the RV signal, using a Markov Chain Monte Carlo (MCMC). We assume measurement uncertainties are Gaussian and uncorrelated. The model parameters corresponding to the maximum likelihood model and the 68.3% credible intervals are given in Table 3, as well as the median value among a posterior sample for each model parameter. (Note that this set of median values does not correspond to any specific model.)

The uncertainties in the model parameters are found using the corresponding posterior distributions from the MCMC. After rejecting the first $\sim 20\%$ of the chain, the values for each of the model parameters were sorted and the smallest and largest 15.9% of the values were rejected. The mean difference between the median of the remaining values for each parameter and the largest and smallest values is our estimate for the uncertainty in that parameter. There is some small asymmetry in the distributions, but it has a sufficiently small effect that we do not report two-sided error bars. In addition, we study the autocorrelation of the chains in the model parameters to determine the uncertainty in our error estimates. The correlation lengths of each parameter indicates a worst-case uncertainty of 10% in the error estimate, while several parameters are much better[1]. The best fitting model and the residuals are shown in Figures 2 and 3 for the eclipse times and RV measurements respectively.

Given the parameter values obtained from the dynamical model, an additional analysis was conducted on the light curve in order to determine the sizes of the stars in the binary. Given that the eclipse depths are almost indistinguishable, we assumed that the two stars are identical in size and mass (with masses equal to $0.212\,M_\odot$). The result of this analysis (also shown in Table 3) is that the radii of the two binary members are $0.28 \pm 0.05 R_\odot$. These radii estimates are somewhat larger than the isochrone models for low-mass stars given in Baraffe et al. (1998), however, the discrepancy is not significant. Moreover, the rather large uncertainty in these sizes makes them less useful for comparison to other measured systems. Additional photometric data from *Kepler* should lessen the uncertainty in this parameter and consequently provide more valuable insight into the physical properties of such stars and our modelling of them.

[1] The relevant quantity being the number of correlation lengths in a Markov chain rather than the number of links in the chain.

Table 3. Parameter values for the KOI 928 system

Parameter	Value	Error	Best Fitting
M_3	0.97 ($M_\odot$)	0.1*	0.97
M_{12}	0.424 ($M_\odot$)	0.017†	0.423808
P_{12}	4.988287 (Days)	0.000015	4.988284
P_3	116.03 (Days)	0.35	115.986209
e_3	0.262	0.013	0.263156
τ_3	121.21 (Days)	0.83	121.192538
ϖ_3	5.195 (rad)	0.075	5.175702
T_0	66.4219 (Days)	0.0016	66.422127
$v_{\rm offset}$	-560 (m/s)	240	-612.095406
$R_1 (= R_2)$	0.28 ($R_\odot$)	0.05	–‡

* This quantity was held fixed during the dynamical analysis and the stated error comes from a separate analysis of the stellar spectrum.
† This is the formal uncertainty from the MCMC analysis. The true uncertainty would be much larger due to the uncertainty in the mass of the tertiary.
‡ This quantity is not part of the dynamical model.

5 DISCUSSION

Eclipse time measurements and their counterparts in the field of transiting exoplanets provide very precise measurements of the orbital phase of the various bodies. Consequently, eclipse and transit times can be used to make similarly precise measurements of the various mass ratios and orbital parameters in multi-object systems. In many cases the values of some parameters derived from timing measurements are significantly more precise than corresponding values from radial velocity measurements (the orbital period, for example). Similarly, some parameters are more difficult to determine from timing measurements—depending upon the orbital configuration—such as the argument of pericentre ϖ_3.

Regardless, with the high precision photometry enabled by the *Kepler* spacecraft, dynamical studies of multi-object systems through timing variations has proven extremely useful as a tool to measure the orbital properties of these systems and the masses of the objects within them. Striking examples include the planetary systems Kepler-9 (Holman et al. 2010) and Kepler-11 (Lissauer et al. 2011) as well the hierarchical triple star KOI 126 (Carter et al. 2011) and now KOI 928.

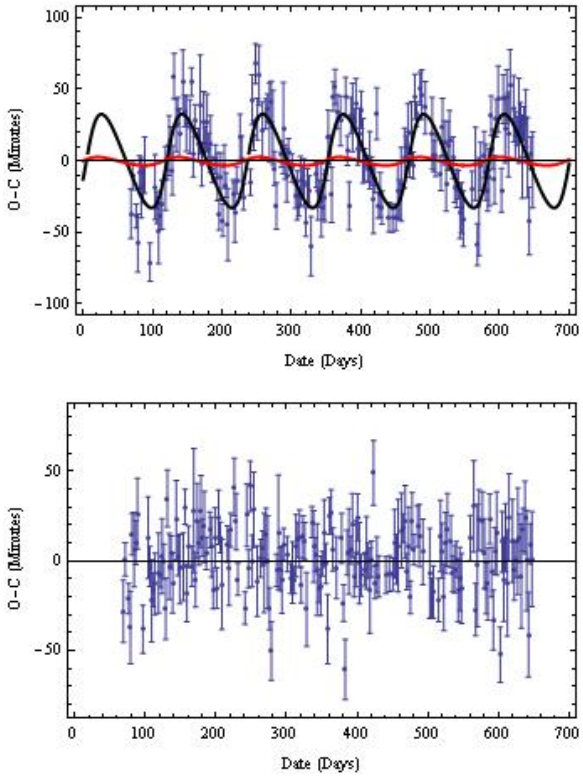

Figure 2. (Top) Plot of the timing data and the best fitting model. A second (barely visible) red curve shows the LTT effect which is the only means to measure the orbital orientation ϖ_3 without RV measurements. (Bottom) Residuals after subtracting the model transit times.

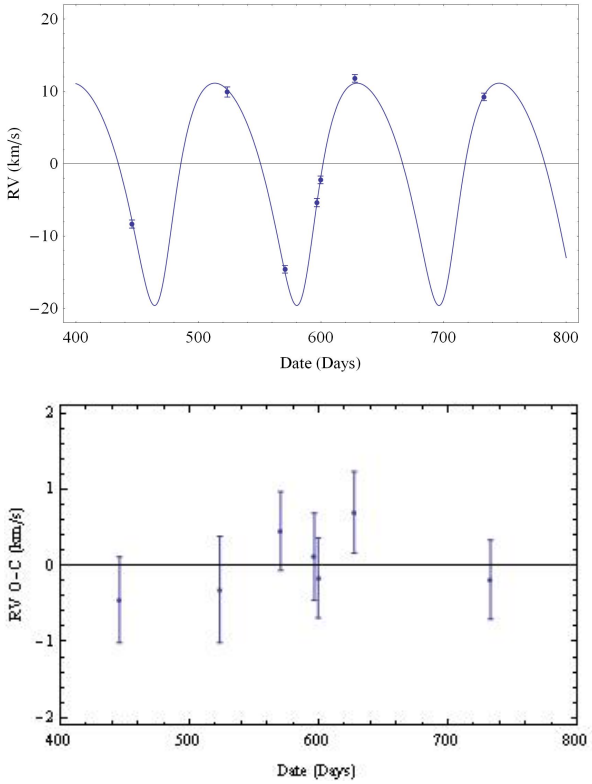

Figure 3. (Top) Plot of the RV data and the best fitting model. (Bottom) Residuals after subtracting the model transit times.

For both KOIs 928 and 126 the very small masses determined by the dynamical analysis provide important guidance to stellar models at the low-mass end of the main sequence. The masses in both KOI 928 and in KOI 126 are among the smallest masses observed in binary systems. Future investigations of multiple star systems through eclipse timing variations, especially with *Kepler* photometry are likely to yield an important sample of these systems with configurations and masses heretofor unexplored.

APPENDIX: TABLE OF ECLIPSE TIMES

ACKNOWLEDGMENTS

Kepler is NASA's tenth Discovery mission with funding provided by NASA's Science Mission Directorate. D. C. F. acknowledge NASA support through Hubble Fellowship grants #HF-51272.01-A and #HF-51267.01-A, awarded by STScI and operated by AURA under contract NAS 5-26555.

REFERENCES

E. Agol, J. Steffen, R. Sari, and W. Clarkson. *MNRAS*, 359:567–579, May 2005.

I. Baraffe, G. Chabrier, F. Allard, and P. H. Hauschildt. *A & A*, 337:403–412, September 1998.

T. Borkovits, B. Érdi, E. Forgács-Dajka, and T. Kovács. *A&A*, 398:1091–1102, February 2003.

L. A. Buchhave et al. *ApJ*, 720:1118–1125, September 2010.

L. A. Buchhave et al. in preparation. 2011.

J. Carter et al. *Science*, 307:1288–1291, February 2011.

A. A. Djupvik and J. Andersen. pages 211–+, 2010.

D. Fabrycky. *Detection and dynamics of transiting exoplanets, Observatiore do Haute Provence*, 2010.

M. J. Holman and N. W. Murray. *Science*, 307:1288–1291, February 2005.

M. J. Holman et al. *Science*, 330:51–, October 2010.

J. M. Jenkins et al. volume 7740 of *Society of Photo-Optical Instrumentation Engineers (SPIE) Conference Series*, July 2010.

D. G. Koch et al. *ApJL*, 713:L79–L86, April 2010.

R. L. Kurucz. volume 149 of *IAU Symposium*, pages 225–+, 1992.

J. J. Lissauer et al. *Nature*, 470:53, January 2011.

K. Mandel and E. Agol. *ApJL*, 580:L171–L175, December 2002.

D. L. Nidever, G. W. Marcy, R. P. Butler, D. A. Fischer, and S. S. Vogt. *ApJS*, 141:503–522, August 2002.

A. Prša and T. Zwitter. *ApJ*, 628:426–438, July 2005.

R. W. Slawson et al. *ArXiv e-prints*, March 2011.

G. Torres et al. *ApJ*, 727:24–+, January 2011.

H. Wu et al. volume 7740 of *Society of Photo-Optical Instrumentation Engineers (SPIE) Conference Series*, July 2010.

Table 4. Primary eclipse times used in the analysis of this system. The uncertainties are in days and date is BJD – 2454900.

Epoch	Date	Uncertainty	Epoch	Date	Uncertainty
0	68.911201	0.012018	58	358.240906	0.013397
2	78.873566	0.014027	59	363.281555	0.008515
3	83.888573	0.014472	62	378.241272	0.009688
4	88.888039	0.013648	63	383.176941	0.011676
7	103.842087	0.015819	64	388.208099	0.016539
8	108.809212	0.015918	65	393.203339	0.012011
9	113.810135	0.011952	66	398.176483	0.012884
10	118.81118	0.015405	67	403.156799	0.015741
11	123.815392	0.014478	69	413.128784	0.014025
12	128.791595	0.011868	70	418.098053	0.016432
13	133.801773	0.012774	71	423.12796	0.012527
14	138.786362	0.011677	72	428.076874	0.010739
15	143.799454	0.015389	77	453.020203	0.013291
16	148.767578	0.013429	78	458.011719	0.017929
17	153.754303	0.013067	79	463.012665	0.014529
18	158.729309	0.011143	80	468.013245	0.01409
20	168.729935	0.024025	81	473.001129	0.015396
21	173.70993	0.014521	82	478.007233	0.010852
22	178.697556	0.013952	84	487.984894	0.012072
23	183.675522	0.013818	85	492.966827	0.012657
25	193.636154	0.0116	87	502.930939	0.017502
26	198.624512	0.011541	88	507.90863	0.01025
27	203.617828	0.010471	90	517.898987	0.013851
28	208.577942	0.017487	91	522.859192	0.012841
30	218.560303	0.014438	92	527.869263	0.014128
32	228.562958	0.010952	93	532.848816	0.010089
35	243.556519	0.012086	94	537.822205	0.009151
36	248.56221	0.009725	95	542.79834	0.01213
37	253.544861	0.014524	96	547.783997	0.013464
38	258.5065	0.013676	100	567.72467	0.010141
39	263.502747	0.007326	101	572.750916	0.011728
40	268.487061	0.019154	102	577.744812	0.011363
41	273.472717	0.017923	103	582.715576	0.00987
42	278.422852	0.011309	104	587.740295	0.00963
44	288.437225	0.022191	105	592.697571	0.011524
45	293.40271	0.012995	106	597.724915	0.016151
48	308.357758	0.011893	107	602.669006	0.010604
49	313.352875	0.0121	108	607.686768	0.016118
50	318.340729	0.011106	109	612.672607	0.020504
51	323.327301	0.008211	111	622.648499	0.011646
52	328.286224	0.014265	112	627.644287	0.020589
54	338.289398	0.013852	113	632.61499	0.020151
55	343.273407	0.017753	114	637.621765	0.014057
56	348.262726	0.011482	115	642.560303	0.016378
57	353.280609	0.013004	116	647.573486	0.018376

This paper has been typeset from a TEX/ LATEX file prepared by the author.

Table 5. Secondary eclipse times used in the analysis of this system. The uncertainties are in days and date is BJD – 2454900.

Epoch	Date	Uncertainty	Epoch	Date	Uncertainty
0.5	71.423409	0.006498	58.5	360.782715	0.007054
1.5	76.392502	0.00588	59.5	365.763611	0.008296
2.5	81.402039	0.008043	60.5	370.747498	0.012001
3.5	86.383942	0.008512	62.5	380.709595	0.007119
5.5	96.323235	0.009293	63.5	385.715057	0.008714
7.5	106.326385	0.007729	64.5	390.701111	0.005317
8.5	111.310364	0.006473	65.5	395.675171	0.007651
10.5	121.309601	0.004985	66.5	400.682617	0.009007
11.5	126.311958	0.006765	67.5	405.644043	0.007943
12.5	131.331589	0.01102	68.5	410.630402	0.006404
13.5	136.303024	0.006376	69.5	415.617615	0.006804
15.5	146.279373	0.00769	70.5	420.602356	0.006952
17.5	156.270187	0.006814	71.5	425.577698	0.006294
18.5	161.239426	0.007947	72.5	430.564819	0.007979
19.5	166.216278	0.007817	74.5	440.536743	0.007105
20.5	171.195129	0.010561	75.5	445.524628	0.006919
21.5	176.193253	0.008447	76.5	450.513214	0.006315
22.5	181.179413	0.007294	77.5	455.510071	0.009652
23.5	186.157288	0.006237	79.5	465.511963	0.005533
24.5	191.150574	0.006963	80.5	470.492767	0.007039
25.5	196.111954	0.007402	81.5	475.479889	0.006334
26.5	201.097565	0.00778	82.5	480.49292	0.00597
27.5	206.10289	0.005941	83.5	485.493591	0.007924
29.5	216.075058	0.007029	87.5	505.414032	0.007591
30.5	221.070267	0.006524	89.5	515.38208	0.008315
31.5	226.0793	0.011133	90.5	520.385315	0.010596
32.5	231.038559	0.006171	91.5	525.372253	0.011837
34.5	241.022278	0.006232	93.5	535.328247	0.007012
35.5	246.033356	0.007357	94.5	540.318115	0.006934
36.5	251.029495	0.010043	95.5	545.295166	0.012277
39.5	265.999756	0.006732	98.5	560.269043	0.008803
40.5	270.991089	0.009914	99.5	565.269775	0.017692
41.5	275.947021	0.008132	100.5	570.237183	0.02373
43.5	285.930481	0.006291	102.5	580.230408	0.013571
44.5	290.914825	0.008349	103.5	585.216187	0.01391
45.5	295.908386	0.006239	104.5	590.21814	0.00964
46.5	300.888611	0.006748	105.5	595.221619	0.009139
47.5	305.86322	0.005782	107.5	605.207397	0.01174
48.5	310.847107	0.00527	108.5	610.196777	0.013152
49.5	315.847626	0.006766	109.5	615.191162	0.016818
50.5	320.815552	0.006921	110.5	620.16748	0.016078
51.5	325.818909	0.00729	111.5	625.14502	0.007044
53.5	335.803284	0.00605	112.5	630.137756	0.009316
54.5	340.782318	0.006592	113.5	635.125061	0.008281
55.5	345.763702	0.005504	114.5	640.097046	0.019446
56.5	350.77002	0.004739	115.5	645.087463	0.007803
57.5	355.767761	0.007724	-	-	-